Manuscript prepared for Atmos. Chem. Phys.
with version 2014/07/29 7.12 Copernicus papers of the LaTeX class copernicus.cls.
Date: 19 April 2015

Development of a custom OMI NO_2 data product for evaluating biases in a regional chemistry transport model

G. Kuhlmann[1,2], Y. F. Lam[1,3], H. M. Cheung[1], A. Hartl[1], J. C. H. Fung[4], P. W. Chan[5], and M. O. Wenig[6]

[1]School of Energy and Environment, City University of Hong Kong, Hong Kong, China
[2]Empa, Swiss Federal Laboratories for Materials Science and Technology, Dübendorf, Switzerland
[3]Guy Carpenter Asia-Pacific Climate Impact Centre, School of Energy and Environment, City University of Hong Kong, Hong Kong, China
[4]Department of Mathematics, The Hong Kong University of Science & Technology, Hong Kong, China
[5]Hong Kong Observatory, Hong Kong, China
[6]Meteorologisches Institut, Ludwig-Maximilians-Universität, Munich, Germany

Correspondence to: G. Kuhlmann (gerrit.kuhlmann@my.cityu.edu.hk) and Y. F. Lam (yunflam@cityu.edu.hk)

Abstract. In this paper, we present the custom Hong Kong NO_2 retrieval (HKOMI) for the Ozone Monitoring Instrument (OMI) on board the Aura satellite which was used to evaluate a high-resolution chemistry transport model (CTM) ($3\,\mathrm{km} \times 3\,\mathrm{km}$ spatial resolution). The atmospheric chemistry transport was modelled in the Pearl River Delta (PRD) region in southern China by the Models-3 Community Multiscale Air Quality (CMAQ) modelling system from October 2006 to January 2007. In the HKOMI NO_2 retrieval, tropospheric air mass factors (AMF) were recalculated using high-resolution ancillary parameters of surface reflectance, a priori NO_2 and aerosol profiles of which the latter two were taken from the CMAQ simulation. We tested the influence of the ancillary parameters on the data product using four different aerosol parametrizations. Ground level measurements by the PRD Regional Air Quality Monitoring (RAQM) network were used as additional independent measurements.

The HKOMI retrieval increases estimated tropospheric NO_2 vertical column densities (VCD) by $(+31 \pm 38)\,\%$, when compared to NASA's standard product (OMNO2-SP), and improves the normalised mean bias (NMB) between satellite and ground observations by 26 percentage points from -41 to $-15\,\%$. The individual influences of the parameters are $(+11.4 \pm 13.4)\,\%$ for NO_2 profiles, $(+11.0 \pm 20.9)\,\%$ for surface reflectance and $(+6.0 \pm 8.4)\,\%$ for the best aerosol parametrisation. The correlation coefficient r is low between ground and satellite observations ($r = 0.35$). The low r and the remaining NMB can be explained by the low model performance and the expected differences when comparing point measurements with area-averaged satellite observations.

The correlation between CMAQ and the RAQM network is low ($r \approx 0.3$) and the model underestimates the NO_2 concentrations in the north-western model domain (Foshan and Guangzhou). We compared the CMAQ NO_2 time series of the two main plumes with our best OMI NO_2 dataset (HKOMI-4). The model overestimates the NO_2 VCDs by about 15 % in Hong Kong and Shenzhen, while the correlation coefficient is satisfactory ($r = 0.56$). In Foshan and Guangzhou, the correlation is low ($r = 0.37$) and the model underestimates the VCDs strongly (NMB $= -40$ %). In addition, we estimated that the OMI VCDs are also underestimated by about 10 to 20 % in Foshan and Guangzhou because of the influence of the model parameters on the AMFs.

In this study, we demonstrate that the HKOMI NO_2 retrieval reduces the bias of the satellite observations and how the dataset can be used to study the magnitude of NO_2 concentrations in a regional model at high spatial resolution of $3 \times 3\,km^2$. The low bias was achieved with recalculated AMFs using updated surface reflectance, aerosol profiles and NO_2 profiles. Since unbiased concentrations are important, for example, in air pollution studies, the results of this paper can be very helpful in future model evaluation studies.

1 Introduction

Nitrogen oxides ($NO_x = NO + NO_2$) play an important role in atmospheric chemistry. As precursors of ozone and aerosols, they are vital in the formation of photochemical smog (Haagen-Smit, 1952) and acid rain (Driscoll et al., 2001). In the troposphere, NO_2 concentrations have a high spatial and temporal variability due to their short lifetime and the variety of sources and sinks. This spatiotemporal variability has been studied with chemistry transport models (CTM), air quality monitoring networks and satellite instruments (e.g. Beirle et al., 2003; Huijnen et al., 2010; Han et al., 2011; Chan et al., 2012; Han et al., 2015; Mueller et al., 2015).

The first satellite instrument able to detect tropospheric NO_2 was the Global Ozone Monitoring Experiment (GOME) which was launched on board the second European Remote Sensing satellite (ERS-2) in 1995 (Burrows et al., 1999). Successor instruments to GOME (GOME-2) are payload on the MetOp satellites used for operational meteorology (Callies et al., 2000). In 2006, the Scanning Imaging Absorption Spectrometer for Atmospheric Cartography (SCIAMACHY) was launched on board the ENVIronmental SATellite (ENVISAT) (Bovensmann et al., 1999) and in 2004, the Ozone Monitoring Instrument (OMI) was launched on board the Aura satellite (Levelt et al., 2006). Since the launch of GOME, the spatial resolution of the instruments increased rapidly. While GOME had a smallest ground pixel size of $40\,km \times 320\,km$, that was suitable for coarse global analyses, OMI has a smallest ground pixel size of $13\,km \times 24\,km$. The higher spatial resolution makes OMI applicable for the study of NO_2 in large metropolitan areas.

The OMI NO_2 standard products are the NASA standard product (OMNO2, Version 2.1) (Bucsela et al., 2006, 2013) and the Derivation of OMI tropospheric NO_2 product (DOMINO, Version 2.0)

(Boersma et al., 2007, 2011). The NO_2 retrieval algorithms use ancillary parameters, such as surface reflectance, a priori NO_2 profiles, and aerosol and cloud information, to calculate air mass factors (AMF). The AMFs convert the retrieved NO_2 slant column densities (SCD) to vertical column densities (VCD). In the standard products, a priori NO_2 profiles are taken from global CTMs with a spatial resolution of $2^\circ \times 2.5^\circ$(OMNO2) and $2^\circ \times 3^\circ$(DOMINO). Surface reflectances are taken from an OMI climatology with a spatial resolution of $0.5^\circ \times 0.5^\circ$(Kleipool et al., 2008).

Since NO_2 profile and surface reflectance have a large impact on the NO_2 VCD, the standard products are not directly suitable to study VCDs on a scale below the resolution of these ancillary parameters. However, when more accurate NO_2 profiles are available, for example in model evaluation studies, the VCDs can be corrected using scattering weights (SW) or averaging kernels (AK). The correction removes the dependency on the a priori profile and can be applied either to the OMI NO_2 VCDs or the model profiles (for details see Eskes and Boersma, 2003; Boersma et al., 2005). SW and AK are closely related to vertically resolved AMFs and are provided with the standard products. AKs have been applied, for instance, by Herron-Thorpe et al. (2010), who validated the regional-scale air quality model AIRPACT-3 ($12\,\mathrm{km} \times 12\,\mathrm{km}$ spatial resolution) over the Pacific Northwest, and Zyrichidou et al. (2013), who evaluated the Comprehensive Air Quality Model (CAMx) ($10\,\mathrm{km} \times 10\,\mathrm{km}$) over Southeastern Europe. Applying AKs has a large influence on the magnitude of tropospheric NO_2 VCDs (Herron-Thorpe et al., 2010).

In the standard products, AKs and SWs depend on the OMI surface reflectance climatology. The spatial resolution of this climatology is coarse compared to the OMI ground pixel size. Therefore, customised NO_2 products have been developed which recalculate AKs, and thus AMFs, using high-resolution surface reflectance products (Zhou et al., 2010; Russell et al., 2011; McLinden et al., 2014). Furthermore, AKs and SWs are affected by aerosols directly due to additional scattering and absorption (Leitão et al., 2010) as well as indirectly due to their impact on the retrieval of surface reflectance and cloud properties (Boersma et al., 2011; Lin et al., 2014). Since the ancillary parameters have a large impact on the magnitude of the retrieved NO_2 VCDs, it is important to consider their influence, for example, in air pollution studies where unbiased pollutant concentrations are important.

For this paper, we developed a customized OMI NO_2 retrieval and applied it to the Pearl River Delta (PRD) region in southern China. The Hong Kong OMI (HKOMI) retrieval recalculates tropospheric AMFs and uses them with OMNO2 SCDs to calculate VCDs. The HKOMI product was used to evaluate the Models-3 Community Multiscale Air Quality (CMAQ) modelling system ($3\,\mathrm{km} \times 3\,\mathrm{km}$ spatial resolution) (Byun and Schere, 2006). The study period is October 2006 to January 2007. Three automatic weather stations and sixteen ground level stations of the PRD Regional Air Quality Monitoring (RAQM) network were used to validate model and retrieval. The objective is to estimate the influence of the ancillary parameters on the evaluation and to demonstrate some possibilities and limitations for using satellite-based NO_2 observations.

This paper is organised as follows: OMI and the retrieval of tropospheric NO_2 including the AMF calculations using the SCIATRAN radiative transfer model are described in Sect. 2. The RAQM network, the CMAQ model run and the HKOMI NO_2 retrieval are described in Sect. 3. The results are presented in Sect. 4 and discussed in Sect. 5. Finally, Sect. 6 concludes this paper.

2 Background

2.1 Ozone Monitoring Instrument (OMI)

OMI is a nadir-viewing imaging spectrometer measuring Earth's reflectance spectra in the near-ultraviolet and visible wavelength range with two charge-coupled device (CCD) arrays. It was launched aboard NASA's EOS Aura satellite on 15 July 2004 (Levelt et al., 2006). The instrument provides near daily global coverage at an overpass time of $13{:}45 \pm 15$ minutes local time (LT). Earth reflectance spectra are measured during the sunlit part of about 14.5 sun-synchronous orbits per day. Trace gases, such as ozone (O_3), sulfur dioxide (SO_2) and nitrogen dioxide (NO_2), are retrieved from the reflectance spectra as well as cloud and aerosol properties. The measurement principle is an along-track (push-broom) scanner with a swath width of 2600 km which is divided into 60 pixels. The ground pixel size varies between $13\,\mathrm{km} \times 24\,\mathrm{km}$ at nadir and $40\,\mathrm{km} \times 160\,\mathrm{km}$ at the swath edge (Levelt et al., 2006). Since June 2007, OMI is affected by a row anomaly which reduces the number of valid measurements (see http://www.knmi.nl/omi/research/product/rowanomaly-background.php for details).

2.2 Standard retrieval of tropospheric NO_2 column densities

The OMNO2 product is the basis for the HKOMI retrieval. Therefore, we give a brief introduction to their algorithm. The OMNO2 retrieval algorithm has three major steps:

1. The total slant column densities S are obtained from the reflectance spectra using the differential optical absorption spectroscopy (DOAS) technique (Platt and Stutz, 2008).
2. The stratospheric slant column densities S_{strat} are subtracted from the total column S using a stratosphere–troposphere separation (STS) algorithm (Bucsela et al., 2013).
3. The tropospheric slant column densities S_{trop} are converted to vertical column density V_{trop} using a tropospheric air mass factors (AMF) A_{trop} (Palmer et al., 2001).

The AMF is defined as the ratio of slant and vertical column density (Solomon et al., 1987). Thus the tropospheric column density V_{trop} is calculated by

$$V_{\text{trop}} = \frac{S - S_{\text{strat}}}{A_{\text{trop}}} = \frac{S_{\text{trop}}}{A_{\text{trop}}}. \tag{1}$$

The tropospheric AMF depends on parameters such as sun position, instrument viewing direction, surface reflectance, atmospheric scattering properties due to air molecules, aerosols and clouds, and

the a priori NO_2 profile. It is related to the vertical sensitivity of the satellite instrument and can be computed for N vertical layers by

$$A_{\text{trop}} = \frac{\sum_{k=1}^{N} \alpha_k \, m_k \, V_k}{\sum_{k=1}^{N} V_k} \tag{2}$$

with:

- α_k: an empirical temperature correction coefficient accounting for the temperature dependency of the NO_2 absorption cross section,
- m_k: the differential or box air mass factor which describes the instrument sensitivity for layer k,
- V_k: the partial NO_2 VCD of layer k.

The products $\alpha_k m_k$ are the scattering weights provided with the standard product. The correction coefficient α_k can be computed by the empirical formula

$$\alpha_k = 1 - 0.003\,\mathrm{K}^{-1}(T_k - T_{\text{ref}}) \tag{3}$$

where T_k is the temperature in layer k and T_{ref} is reference temperature of the NO_2 absorption cross section ($T_{\text{ref}} = 220\,\mathrm{K}$) (Bucsela et al., 2013).

The box air mass factors m_k can be computed with a radiative transfer model. The OMNO2 algorithm uses the TOMRAD radiative transfer model (Dave, 1965). The AMF formulation used in OMNO2 is based on a AMF formulation by Palmer et al. (2001). In partly cloudy scenes, OMNO2 computes the box AMFs using the independent pixel approximation (IPA). The approximation calculates AMFs as weighted sums of a cloudy m_k^{cloudy} and a clear m_k^{clear} component:

$$m_k = w \cdot m_k^{\text{cloudy}} + (1 - w) \cdot m_k^{\text{clear}}, \tag{4}$$

where w is the aerosol/cloud radiance fraction (CRF), that is the fraction of measured radiation that results from clouds and aerosols (Acarreta et al., 2004).

In OMNO2, the partial VCD V_k are taken from the Global Modeling Initiative (GMI) CTM (Duncan et al., 2007; Strahan et al., 2007) which combines stratospheric chemistry described by Douglass et al. (2004) and tropospheric O_3-NO_x-hydrocarbon chemistry from the GEOS-Chem model (Bey et al., 2001). It should be noted that, for an optical thin absorber, only the relative shape of the profile $n_k = V_k / V_{\text{trop}}$ is required for the AMF calculation.

Bucsela et al. (2013) estimated tropospheric NO_2 VCD uncertainties to be $1 \times 10^{15}\,\mathrm{cm}^{-2}$ for clear skies and up to $3 \times 10^{15}\,\mathrm{cm}^{-2}$ for large cloud radiance fractions. In polluted regions, the main uncertainties are the DOAS fit (10 % relative error) and the tropospheric AMFs (20–80 %).

2.3 SCIATRAN radiative transfer model

SCIATRAN is a one-dimensional RTM which can be used for the calculation of box AMFs (Rozanov et al., 2005). The model is designed as a forward model for the retrieval of atmospheric constituents from measurements of scattered light by satellite, ground or airborne instruments. The wavelength range goes from 175 to 2380 nm which includes the ultra violet, visible and near infra-red part of the spectrum.

SCIATRAN solves the integro-differential radiative transfer equation using the discrete-ordinates method (DOM) in the plane-parallel or pseudo-spherical mode to calculate box AMF profiles. Box AMFs m_k are derived from weighting functions which describe the sensitivity of the reflectance spectrum R to a perturbation of a model parameter Δn in layer z_k. In SCIATRAN, weighting functions are computed by a quasi-analytic approach (Rozanov et al., 1998). If Δn is a perturbation of the $\mathrm{NO_2}$ number density n_k, the box AMF m_k is the negative weighting function (Rozanov and Rozanov, 2010).

3 Methodology

In this section, we describe the RAQM network, the CMAQ CTM and the HKOMI retrieval. Our study period is from October 2006 to January 2007 which has been chosen because cloud fractions in the PRD region are lowest in this season and OMI measurements in later years are affected by the aforementioned row anomaly.

3.1 Ground networks

3.1.1 Meteorological observations

Meteorological observations were used for the evaluation of the simulated meteorological fields which were used to drive the CTM. The data were measured by three automatic weather stations in Hong Kong. The stations are located at the Hong Kong Observatory (HKO) headquarters, the Hong Kong International Airport (HKIA) and on Waglan Island (WGL) (see Fig. 1). HKO is in the city centre of Kowloon and surrounded by high buildings. HKIA is located on an artificial island near Tung Chung to the north of mountainous Lantau Island. Waglan Island is a small island located to the east of Hong Kong Island. The island is too small to be resolved by the model grid. The WGL station is located 56 m above sea level and used as background station by the Hong Kong Observatory. The used meteorological parameters are hourly measurements of temperature (T), humidity (q), sea surface pressure (p) and wind (v). Temperature and humidity have been measured at 2 m above ground level (a.g.l.).

3.1.2 Pearl River Delta Regional Air Quality Monitoring Network

Ground-level NO_2 mixing ratios were provided by the RAQM network. The network was established by the governments of the Guangdong province and Hong Kong to monitor the air quality in the PRD region and has been in operation since 30 November 2005. It consists of sixteen automatic air quality monitoring stations (see Fig. 1, round markers). The network measures NO_2, SO_2, O_3 and PM_{10} hourly. The monitoring network was used to validate the NO_2 mixing ratios of the OMI NO_2 products and the CMAQ simulation. In the network, NO_2 is measured by chemiluminescence and DOAS technique with an accuracy and precision of about 10 % (GDEMC and HKEPD, 2006).

3.2 CMAQ model simulation

Atmospheric chemistry was simulated with the CMAQ modelling system version 4.7.1 (Byun and Schere, 2006). Three model domains were defined using a Lambert conformal conic projection (Fig. 1). The coarse domain (D1) covers East Asia with a spatial resolution of $27\,\mathrm{km} \times 27\,\mathrm{km}$. The nested domains have grid resolutions of $9\,\mathrm{km} \times 9\,\mathrm{km}$ (D2) and $3\,\mathrm{km} \times 3\,\mathrm{km}$ (D3), respectively.

Meteorological fields were provided by the Weather Research and Forecasting (WRF) modelling system (Skamarock et al., 2008) driven by NCEP Final Analysis (FNL) data (NCEP et. al., 1997). Horizontal advection was modelled with the mass-conserving YAMO scheme (Yamartino, 1993). The default vertical advection scheme was replaced by the new advection scheme implemented in CMAQ version 5.

The gas-phase chemistry was modelled with the Euler backward iterative solver optimized for the Carbon Bond-05 mechanism with chlorine (Yarwood et al., 2005). Aerosol chemistry was modelled with the fifth-generation CMAQ aerosol model (aero5) while the impact of clouds on deposition, mixing, photolysis, and aqueous chemistry was set by the Asymmetrical Convective Model (ACM) cloud processor (Pleim and Chang, 1992). Three-dimensional extinction coefficients were computed by the empirical IMPROVE formula (Malm et al., 1994).

The emission inventory used in this simulation was compiled by Du (2008). The inventory combines monthly anthropogenic emission from INTEX-B (Zhang et al., 2009) with biogenic emissions from GEIA (Global Emissions Inventory Activity, Guenther et al., 1995), and biomass burning and ship emissions from TRACE-P (Streets et al., 2003). The INTEX-B emissions were updated with regional emissions for Hong Kong provided by the Hong Kong Environmental Protection Department.

Model outputs used were hourly ground level values and three-dimensional fields of NO_2 mixing ratios, aerosols and meteorological parameters averaged from 13:00 to 15:00 LT (OMI overpass time). In addition, at each ground station, time series of hourly meteorological parameters and NO_2 mixing ratios were extracted from the model output. The surface pressure in the model was converted to sea level pressure using the simulated temperature. The wind vector in the model was taken at the

height of the measurement stations to account for the elevation of the stations above averaged surface height.

3.3 The Hong Kong OMI (HKOMI) NO_2 retrieval

For the HKOMI NO_2 retrieval, we recalculated tropospheric AMFs with Eq. (2) with new ancillary parameters. The new AMFs were used to compute the tropospheric VCDs with Eq. (1).

For the AMF calculation, a set of ancillary parameters was compiled for each OMI ground pixel. The parameters were taken mainly from the WRF/CMAQ simulation. Thus, the retrieval does not depend on any other CTM model which makes the model evaluation easier. The parameters are surface elevations, temperature, pressure and NO_2 profiles, as well as aerosol extinction coefficients. Further ancillary parameters are cloud height and CRF, which were taken from the OMI O_2-O_2 cloud product (Acarreta et al., 2004), and surface reflectance, which was taken from the MODIS MCD43C2 product (Wanner et al., 1997; Lucht et al., 2000).

All ancillary parameters were projected to a $0.01^\circ \times 0.01^\circ$ (about $1\,\mathrm{km} \times 1\,\mathrm{km}$) longitude–latitude grid and then averaged to each OMI ground pixel. The grid points were weighted based on the instrument's spatial sensitivity within the pixel boundaries (Dobber et al., 2006; Kurosu and Celarier, 2010), in contrast to other custom retrievals, where each grid point was given equal weight.

We recalculated temperature correction coefficients $\alpha_k(T_k)$, box AMFs m_k and partial VCDs V_k. The temperature correction coefficients $\alpha_k(T_k)$ were calculated by Eq. (3) from the WRF/CMAQ output. The box AMFs were computed with the SCIATRAN radiative transfer model. The partial VCDs were also calculated from the WRF/CMAQ output. As an example, two NO_2 profiles are shown in Fig. 2.

3.3.1 Surface reflectance

The surface reflectance was calculated from the MODIS MCD43C2 product. The product is available every eight days compiled from 16 days of data. The spatial resolution is $0.05^\circ \times 0.05^\circ$ (Wanner et al., 1997; Lucht et al., 2000). We calculated the black-sky albedo (BSA) from the polynomial representation of the bidirectional reflectance distribution function (BRDF) using solar zenith angle (SZA) and model parameters for MODIS Band 3 (Lucht et al., 2000). MODIS Band 3 has a wavelength range from 459 to 479 nm and a centre wavelength of 470 nm. This band is closest to the DOAS fitting window used in the NO_2 retrieval (405–465 nm). Systematic errors due to the wavelength inconsistency are expected to be small. The MODIS surface reflectance has been used in other custom OMI NO_2 products (Zhou et al., 2010; Russell et al., 2011; Lin et al., 2014; McLinden et al., 2014).

Since the BSA model parameters have missing values due to cloud contamination, Zhou et al. (2010) filled the data gaps by applying a series of spatial and temporal interpolations. They also reduced measurement noise by applying a smoothing filter. In this work, we combined their steps by

using normalised convolution which is a useful algorithm for filling missing values (Knutsson and Westin, 1993). We used a three-dimensional, uniform kernel of size 5 to fill the gaps in the model parameters. The BSA was calculated from the model parameters for each OMI ground pixel.

3.3.2 Aerosols and clouds

Scattering by aerosols and clouds affects the AMF (Leitão et al., 2010). Aerosol scattering at or below an $\mathrm{NO_2}$ layer increases the AMF, but scattering above the $\mathrm{NO_2}$ layer will reduce the AMF. In addition, aerosol optics affects the retrieval of cloud properties.

Clouds are typically handled by the independent pixel approximation (Eq. 4), while aerosols are only treated implicitly in the standard and most custom $\mathrm{NO_2}$ products. In OMNO2, cloud pressure and CRF are taken from the OMI $\mathrm{O_2}-\mathrm{O_2}$ cloud product which is sensitive to weakly absorbing aerosols (Boersma et al., 2011). Aerosols are also included in the OMI surface climatology which includes ground haze and persistent cloud features (Kleipool et al., 2008). Lin et al. (2014) included aerosols from a regional GEOS-Chem simulation. They used aerosol optical thickness (AOT) and assumed different profiles of aerosol extinction and absorption coefficients. They also recalculated the OMI cloud product to remove the aerosol component. Boersma et al. (2011) derived an empirical relationship between MODIS AOT and OMI CRF:

$$\mathrm{CRF} = 0.21 \cdot \mathrm{AOT}. \tag{5}$$

The formula was derived from observations over North America which were cloud free according to the MODIS AOT retrieval but had non-zero CRF according to the OMI retrieval.

In the HKOMI retrieval, we treated clouds as in OMNO2 using the independent pixel approximation. In SCIATRAN, clouds were implemented as an opaque surface at the height of the OMI cloud pressure product with a surface reflectance of 0.8 and the box AMF was calculated with Eq. (4).

Aerosol extinction coefficients can be calculated from the CMAQ output using the empirical IMPROVE formula (Malm et al., 1994). In the standard output, CMAQ calculates only ground level extinction coefficients. In our custom retrieval, we implemented four different aerosol parametrizations:

Case 1: No explicit aerosol treatment, i.e. aerosols were only included implicitly through the OMI cloud product.

Case 2: Aerosols were described by the LOWTRAN aerosol parametrization which requires only very limited information about season, aerosols type, visibility and relative humidity at four different layers: planet boundary layer (PBL) (0–2 km), troposphere (2–10 km), stratosphere and mesosphere. We set the season to autumn/winter and the aerosol type to urban. The PBL visibility was calculated from the CMAQ ground extinction coefficients β using the definition of the meteorological optical range (MOR) (World Meteorological

Organization, 2008):

$$\mathrm{MOR} = -\frac{\log 0.05}{\beta}. \quad (6)$$

The visibility in the free troposphere was set to 23 km. Furthermore, we assumed that no volcanic aerosols were in the stratosphere or mesosphere. The relative humidity in the PBL and the free troposphere were taken from WRF. Visibility and relative humidity were set to the nearest predefined value in the LOWTRAN parametrisation.

Case 3: Vertical profiles of extinction coefficients β were computed from CMAQ output using the IMPROVE formula. The formula includes a constant Rayleigh extinction coefficient of 0.01 which is subtracted to obtain the aerosol extinction coefficient β_{ext}. Since the IMPROVE formula calculates β_{ext} at 550 nm, an Ångström exponent α for urban aerosols is used to calculate extinction coefficients at 435 nm (Hess et al., 1998). Furthermore, a single scattering albedo ω_0 of 0.82 (urban aerosol) in PBL (below 2 km) and 0.93 in free troposphere is used to calculate aerosol absorption coefficients β_{abs}. The phase function is modelled by Henyey–Greenstein parametrisation with an asymmetry factor g of 0.689 (Hess et al., 1998). As examples, two β_{ext} profiles are shown in Fig. 2.

Case 4: Since these three parametrisations include aerosols implicitly through the cloud product, aerosol might be counted twice. Therefore, the CRF was corrected by Eq. (5) using the AOT in CMAQ. This was done mainly because recalculation of the OMI cloud product was outside the scope of our study. Since this formula was derived from cloud free observations over North America, generalisation to cloudy pixels in other regions should be considered with great caution. Otherwise, aerosols were treated as in Case 3.

3.3.3 OMI $\mathrm{NO_2}$ datasets for the PRD region

For our study, we created six OMI $\mathrm{NO_2}$ datasets. The first dataset uses the OMNO2 standard product (OMNO2-SP). For the second dataset (OMNO2-SW), AMFs were recalculated using OMNO2 scattering weights and CMAQ $\mathrm{NO_2}$ profiles. The remaining four datasets were created with our HKOMI retrieval for each aerosol case (HKOMI-1, -2, -3 and -4).

The number of OMI $\mathrm{NO_2}$ VCDs, which allows for the study of the $\mathrm{NO_2}$ distribution, is limited due to two factors. First, the ground pixel size at the end of the swath is very large and thus not suitable for studying the local spatial distribution. Therefore, only the inner fifty out of sixty rows were used in this study. Second, the presence of clouds increases the retrieval uncertainty. Therefore, only ground pixels were used with CRFs smaller than 50 %. Since the CRF is also sensitive to aerosols, this filter criterion is likely to remove heavily polluted days as well. We further removed all orbits that did not have valid pixels in the urbanised area of the model domain (see Fig. 1).

3.4 Data processing

The OMI NO_2 datasets have been compiled in the instrument's frame of reference (level 2). For comparison and visualisation, the datasets need to be projected to the model grid (level 3) using a suitable gridding algorithm. This is not a trivial task, because the algorithm should conserve the NO_2 VCDs within the OMI ground pixels which are overlapping in along-track direction. In this study, we use a new gridding algorithm which reconstructs the spatial distribution using a parabolic spline surface (Kuhlmann et al., 2014, the source code was downloaded at https://github.com/gkuhl/omi). Each orbit was projected to a $0.01^\circ \times 0.01^\circ$ longitude–latitude grid. It would be more plausible to project all data to the CMAQ model grid, but the gridding algorithm code currently only supports longitude–latitude grids.

Since OMI has a lower spatial resolution than the CMAQ simulation, the satellite instrument cannot resolve small features in the simulated NO_2 distribution. In addition, OMI's spatial resolution depends on the current satellite orbit and thus changes from day to day. Therefore, we create a processed CMAQ dataset (CMAQ processed) from the model output (CMAQ raw). The raw CMAQ VCDs were averaged for each OMI ground pixel in an orbit. Then, the CMAQ data were projected back onto a $0.01^\circ \times 0.01^\circ$ longitude–latitude grid using the gridding algorithm (Kuhlmann et al., 2014). In this step, missing OMI pixels were also removed from the CMAQ data. Using this approach, the NO_2 horizontal distributions of OMI and CMAQ are directly comparable.

For each RAQM ground station location, time series of tropospheric NO_2 VCDs were computed from the six OMI datasets. To study the additive and proportional differences, the OMI VCDs were converted to mixing ratios using the CMAQ NO_2 profile shapes. Since many stations are located on top of buildings, the mixing ratios were calculated at the station height using nearest-neighbour interpolation. In addition, these time series were also computed for the processed CMAQ dataset.

3.5 Evaluation study

For our evaluation study, we have six OMI datasets, two CMAQ datasets as well as time series of these datasets at each RAQM station and the measurements of the RAQM stations. Furthermore, we have simulated and measured meteorological parameters at three ground stations. In this paper, we performed the following analyses with these datasets:

- First, we compared the six OMI datasets (level 2) with each other to identify the impact of the ancillary parameters on the tropospheric NO_2 VCDs. We calculated normalised mean bias (NMB) and coefficient of variance (CV) for all valid OMI VCDs in the datasets. Since high NO_2 values are particularly important for air pollution studies, we also calculated NMB and CV for the 10% highest VCDs based on HKOMI-3. Furthermore, we used a standard set of typical ancillary parameters (see Table 1) to obtain a better understanding of the differences between the datasets.

– Second, we compared the WRF/CMAQ time series with the ground network measurements using index of agreement (IOA), Pearson's correlation coefficient r, root mean square error (RMSE), mean bias (MB), CV and NMB (Table 2). In our analysis, we concentrated on two large urban areas which have the highest NO_2 mixing ratios. The first area consists of the Hong Kong area and the Shenzhen prefecture (HKSZ) and the second area consists of the Foshan and Guangzhou prefectures (FSGZ). HKSZ includes the RAQM stations Liyuan, Tap Mun, Tung Chung and Tsuen Wan. FSGZ includes the RAQM stations Huijingcheng, Luhu Park, Shunde Dangxioa and Wanqingsha.

– Third, we validated the OMI datasets (level 3) with ground measurements. The validation with point measurements is challenging, because OMI measures the mean value within the ground pixels ($\geq 13\,\mathrm{km} \times 24\ \mathrm{km}$). Since NO_2 has a high spatial variability, area average and point measurement may not agree well; in particular in an urban area with complex NO_2 sources and sinks. In order to get an idea for the expected deviations, we compared the time series of the processed CMAQ dataset, which have been averaged to the OMI ground pixels, with the raw CMAQ dataset at the 16 stations. Furthermore, if the VCDs are converted to ground values with the CMAQ profile shapes, the validation depends on the modelled NO_2 profiles which can have large uncertainties. This was studied by comparing different NO_2 profiles.

– Finally, OMI and CMAQ datasets were compared to evaluate the regional CTM with the OMI NO_2 products. We studied the spatial distribution of tropospheric NO_2 VCDs in all datasets. Furthermore, time series were analysed for the two urban areas (HKSZ and FSGZ).

4 Results

4.1 OMNO2 and HKOMI NO_2 retrieval

In this subsection, we look at the differences between the six OMI NO_2 datasets. After cloud filtering, 56 days with satellite observations were available covering about 50% of all days in our study period. Figure 3 shows two examples of tropospheric NO_2 distributions (level 2). The spatial distributions are similar between the OMNO2-SP, HKOMI-1 and HKOMI-4 datasets with some differences between individual pixels. On the other hand, NO_2 magnitudes are quite different between the datasets. Figures 4c and e show the averaged NO_2 distribution for whole study period. The averaged OMNO2-SP dataset has a mean value of $0.45 \times 10^{16}\,\mathrm{cm}^{-2}$ and a maximum value of $3.46 \times 10^{16}\,\mathrm{cm}^{-2}$, while the HKOMI-4 dataset has a mean value of $0.59 \times 10^{16}\,\mathrm{cm}^{-2}$ and a maximum value of $5.04 \times 10^{16}\,\mathrm{cm}^{-2}$. The HKOMI-2 dataset has the largest mean ($0.70 \times 10^{16}\,\mathrm{cm}^{-2}$) and maximum value ($5.50 \times 10^{16}\,\mathrm{cm}^{-2}$). Table 3 shows NMB and CV between the datasets for all and the 10% highest VCDs. Since we compared datasets which only differ by one ancillary parameter, the comparison shows the influence of each parameter. CMAQ NO_2 profiles and MODIS surface

reflectance increase VCDs by about 10%. When aerosols were included, VCDs increased between 6 and 24% depending on the parametrisation. If a priori profiles and aerosols are replaced, the increase of the VCDs is larger for the 10% largest VCDs. The HKOMI-4 datasets is 31.0±34.0 % larger than the OMNO2-SP dataset.

In order to assess the differences better, we looked at the influence of the ancillary parameters using typical values. Figure 2 shows a "clean" and "polluted" NO_2 profiles from CMAQ and a profile from GEOS-Chem ($2^\circ \times 2.5^\circ$ spatial resolution) for Hong Kong (Chan et al., 2012). The "polluted" CMAQ NO_2 profile has an AMF of 0.82 and is about 3 % smaller than the "clean" profile (AMF $= 0.84$). The GEOS-Chem profile has an AMF of 1.19 which is 41 % larger than the "clean" and 45 % larger than the "polluted" CMAQ profile. To determine the variance of the AMFs, we calculated the AMFs using all CMAQ profiles. In this sample, the largest AMF is 1.64, due to an elevated NO_2 layer in the upper troposphere, and the smallest AMF is 0.75, due to a heavily polluted ground layer. The sample mean is 0.89 with a standard deviation of 0.08 (about 9% of the mean).

Figure 5a shows the MODIS surface reflectance for a SZA of 48°. On average, the MODIS reflectance is 0.01 ± 0.02 smaller than the OMI reflectance (not shown). The BSA is smaller than the OMI climatology over land but larger over water. In order to identify the improvement due to the higher spatial resolution, we averaged the BSA to the lower spatial resolution used in the standard product ($0.5^\circ \times 0.5^\circ$) and subtracted the high-resolution BSA used in our custom product (Fig. 5b). The distribution shows areas with large differences (up to ±0.03) along the urbanised and likely polluted coastline which would result in large biases (up to ±20 % for a reflectance of 0.05) in the AMF calculation.

Table 4 shows the AMFs for the different aerosol cases using the "clean" and "polluted" profiles (Fig. 2). Cases 3 and 4 are equal because the CRF is zero in the test parameters. The Case 2 AMFs are 19 % smaller than Case 1 for the "clean" and 57 % smaller for the "polluted" aerosol profile. If Case 3 is compared to Case 1, the AMF is reduced between 8 and 14 % (Table 4). In Case 2, the CMAQ ground level extinction coefficient is used as constant coefficient in the PBL (0-2 km). The β_{ext} profiles show that using the ground level extinction coefficient is reasonable for "clean" but not for "polluted" profiles (Fig. 2), because β_{ext} is overestimated above 1 km which reduces the AMF because these artificial aerosols are shading the NO_2 layer below.

4.2 WRF/CMAQ validation with ground measurements

The results of the WRF validation with the automatic weather stations are tabulated in the Supplement (Tab. S1). The IOA between observed and simulated sea level pressure is high (IOA $= 0.99$) at all stations. Simulated temperature and humidity also have high agreement with the observations. The model slightly underestimates temperature and humidity at HKO and HKIA, while it slightly overestimates temperature and humidity at WGL. The agreement between modelled and observed

wind speed is highest at WGL (IOA $= 0.84$), which is located on a remote island, and lower at HKIA (IOA $= 0.68$) and HKO (IOA $= 0.57$), which are located in complex terrain.

The results of the CMAQ validation with the RAQM network are tabulated in the Supplement (Tab. S2). For the sixteen stations, the IOAs have an average of 0.52 and vary between 0.29 (Tap Mun) and 0.75 (Tsuen Wan). The average ground mixing ratios are shown in Fig. 6. In the measurements, two major plumes can be identified in HKSZ and in FSGZ. In the simulations, the FSGZ plume is much less pronounced than in the measurements, which can be seen in the averaged mean bias which is $-17.6\,\mathrm{ppbv}$ ($-44\,\%$) for the four stations in FSGZ. The averaged mean bias is $-0.0\,\mathrm{ppbv}$ ($-5\,\%$) for the stations in HKSZ.

4.3 OMI validation with ground measurements

The comparison between OMI datasets and RAQM stations is impacted by the area averaging effect. The expected error measures were computed by comparing raw and processed CMAQ datasets (Table 5). The expected correlation coefficient is very low (r = 0.25) at HKSZ and good (r = 0.67) at FSGZ. The expected NMBs are -16% and -12% at HKSZ and FSGZ, respectively.

To study additive and proportional differences between satellite and ground observations, the OMI VCDs were converted to ground level mixing ratios using the CMAQ $\mathrm{NO_2}$ profiles. The mean conversion factor ($V_0/(\Delta z_0 V_{\mathrm{trop}})$) is $(1.47 \pm 0.47) \times 10^{-3}\ \mathrm{m^{-1}}$. The conversion factor of the "clean" profiles is about 3% smaller than of the "polluted" profile. The GEOS-Chem profile has a conversion factor of $3.92 \times 10^{-3}\,\mathrm{m^{-1}}$ which is more than twice the factor computed for the CMAQ profiles. As a result, ground level mixing ratios would be much larger if the GEOS-Chem profile would be used for the conversion. The ground mixing ratio map is shown in Fig. 7 for 29 January 2007 using two different gridding algorithms. The algorithm which uses parabolic splines does not show discontinuities at the pixel boundaries and has slightly larger VCDs (Fig. 7b). The $\mathrm{NO_2}$ variability below the OMI pixel size is caused by the variability of the CMAQ profile shapes showing the large impact of the model.

Table 6 shows the statistical measures for the comparison between the six OMI datasets and the ground network. Statistical measures for all 16 stations are tabulated in the Supplement (Table S3) showing that the measures vary considerably between the stations. The averaged correlation coefficients are similar with no large difference between the datasets. At FSGZ, r is smaller than the expected value, while at HKSZ, r is close to the quite small expected value (Table 5). At HKSZ, the HKOMI datasets have a slightly larger correlation coefficient than the two OMNO2 datasets. The datasets largely differ in the mean biases. The bias is largest for the OMNO2-SP and smallest for HKOMI-2 dataset. The bias is closest to the expected bias for the HKOMI-3 and -4 datasets. OMNO2-SP and -SW underestimate $\mathrm{NO_2}$ mixing ratios while HKOMI-2 overestimates the mixing ratios.

4.4 CMAQ evaluation with OMI NO_2 datasets

The modelled NO_2 VCDs were evaluated with the OMI NO_2 datasets. Figures 4a and b show the difference between the raw and the processed CMAQ dataset. In the processed dataset, the spatial NO_2 distribution is smoothed below the size of the OMI ground pixel. Therefore, CMAQ (processed) and OMI datasets can be directly compared without artefacts due to different spatial resolutions.

Table 7 shows the mean values at RAQM stations for CMAQ and OMI datasets. If the model performance would be good, CMAQ (raw) should agree well with RAQM and CMAQ (processed) should agree well with the OMI datasets. The former were already compared in Sect. 4.2 showing a small bias at HKSZ and a large bias at FSGZ. The results are similar between CMAQ (processed) and HKOMI-4 having similar mean values at HKSZ but a large bias at FSGZ.

The NO_2 distribution of the HKOMI-4 dataset has one plume at FSGZ and a second plume at HKSZ (Fig. 4e). In addition, the OMI dataset has increased NO_2 near the northern edge of the model domain and at the Pearl River in the western part of the domain. The differences between CMAQ and OMI are shown in Fig. 4d and f. The modelled VCDs are underestimated at FSGZ and overestimated at HKSZ. The form of the plume at HKSZ differ between OMI and CMAQ. In CMAQ, the plume has an elliptic shape with a strong, south-western outflow. In the OMI datasets, this feature is less distinct.

The results of the time series analysis are shown in Table 8. The correlation coefficient is smaller at FSGZ than at HKSZ. At FSGZ, CMAQ VCDs are much smaller than the HKOMI-4 VCDs (NMB $=$ $-40\,\%$). This bias is close to the bias between CMAQ and RAQM ($-44\,\%$). On the other hand, CMAQ VCDs are larger than the OMI VCDs ($+15\,\%$) at HKSZ.

5 Discussions

5.1 Influence of ancillary parameters

Ancillary parameters have a large influence on the retrieval of tropospheric NO_2 VCDs. In our study, their influence on the AMFs is similar to findings for other retrieval algorithms (e.g. Zhou et al., 2010; Russell et al., 2011; Lin et al., 2014). A direct comparison is difficult because the influence depends on regional factors. For example, we found a very strong gradient in surface reflectance along the coastline in the PRD region which has a large influence on tropospheric NO_2 VCDs. In other regions, the variability of surface reflectance can be smaller influencing VCDs less.

In our retrieval, CMAQ NO_2 profiles were used which have a quite different shape compared to GEOS-Chem profiles (Fig. 2). Since NO_2 profile measurements were not available for the PRD region, the modelled profiles were not validated in this study. As a consequence, AMF uncertainties due to NO_2 profiles are difficult to quantify. However, it can be argued that the regional CMAQ CTM provides more accurate vertical distributions than the global model, because of higher spatial

resolution and more detailed PBL, vertical advection and diffusion schemes. On the other hand, different schemes exist for regional CTM and these might result in different NO_2 profiles (e.g. Tang et al., 2011; Xie et al., 2012). Therefore, the validation of model profiles is important to better estimate the uncertainties for model evaluation with satellite observations. In this study, the CMAQ NO_2 profiles have a strong vertical gradient in the PBL which is expected for strong emissions near the surface. The qualitative shape of the profile agrees reasonable with measured and simulated urban NO_2 profiles used in other studies (e.g. Schaub et al., 2006; Leitão et al., 2010).

Aerosols have a large influence on the retrieved VCDs. In the HKOMI retrieval, good agreement with ground measurements was found when calculating β_{ext} profiles and reducing CRF based on AOT in the model (Case 4). β_{ext} calculation and CRF reduction are based on empirical formulas which have the advantage that they are easy to use. However, the IMPROVE formula was not developed to calculate β_{ext} profiles in an urban environment which can result in uncertainties. An improved IMPROVE formula is available which we consider to use in an updated version of our retrieval (Zhang et al., 2013). Alternatively, optical properties can be calculated by Mie theory. The aerosol information was not validated with ground- or satellite observations which is also planned to be implemented in an updated version. Nevertheless, the shape of the aerosol profiles is in reasonable agreement with LIDAR measurements in Hong Kong (He et al., 2008). The empirical cloud correction formula is also very simple and, as mentioned before, should be improved in future. In conclusion, the impact of aerosols and clouds is an important factor for unbiased retrieval of tropospheric NO_2 VCDs. Unfortunately, a complete treatment of aerosols and clouds is complex and often not feasible for air quality model evaluations.

The OMI surface reflectance climatology provides scene reflectance, which includes both the surface and the presence of boundary layer haze or aerosols, and minimum reflectance, which is the lowest retrieved reflectance value (Kleipool et al., 2008). Since scattering by weakly-absorbing aerosols at or below an NO_2 layer increases AMFs, it has been argued that scene reflectance should be used for satellite-based trace gas retrieval, if no information about aerosols are available (Herman et al., 2001). Furthermore, the minimum reflectance can be underestimated due to ground- and cloud shading or darkening by rainfall. For these reasons, scene reflectance is used in the standard product (Boersma et al., 2011). However, if an NO_2 layer is mixed with highly-absorbing aerosols, the AMF is not increased but decreased (Leitão et al., 2010). In the HKOMI retrieval, we have highly-absorbing ($\omega_0 = 0.82$), urban aerosols and thus AMFs are decreased in the presence of aerosols. As a result, if scene reflectance is used for an urban area, NO_2 VCDs can be strongly underestimated.

Since ancillary parameters have a large influence on the VCDs, it is important to quantify their uncertainties. This is often difficult because vertical profiles are required which are rarely available. In the view of model evaluation, it is also helpful if surface reflectance, aerosols and clouds are provided independently, because it allows to use modelled aerosol profiles in the retrieval.

5.2 WRF/CMAQ validation with ground measurements

The evaluation of the meteorological fields shows good agreement between model and observations within the expected limitations due to the model resolution. The agreement is lower for the wind fields due to the impact of local topography. Unfortunately no meteorological data for the whole PRD region were available. However, due to the high agreement in Hong Kong, similar model performance is expected in the complete model domain. The meteorological fields are sufficient to provide input for the chemistry transport simulations.

The agreement between CMAQ and RAQM network is low for various reasons. First, the point measurement may not be representative for the grid cell because of the influence of local sources and sinks as well as local topography and station height. Second, the differences can arise from the model due to inaccurate wind fields, limited parametrisation of the chemistry and, in particular, insufficient knowledge about strength and distribution of emissions. The model performance is similar to the result by Wu et al. (2012) who also evaluated CMAQ in the PRD region using a similar emission inventory.

The low model performance can largely be explained by problems with the emission inventory. For example, the low IOA at Tap Mun is the result of several peaks in the simulated time series which were not found in the measurements. The peaks were traced back to $\mathrm{NO_x}$ emissions at the Dapend Peninsula about 15 km east of Tap Mun. As a second example, the large bias between model and observations at FSGZ is mainly due to underestimated $\mathrm{NO_x}$ emissions in this region. The smaller bias in HKSZ is thought to be the result of the updated emission inventory with more accurate information for Hong Kong. It should be noted that updated emission inventories exist for the PRD region which would improve the model performance. However, our objective was not an accurate CMAQ simulation but a model evaluation with satellite observations. For this application, the used emissions inventory was found to be very useful.

5.3 OMI validation with ground measurements

The OMI datasets were validated with the RAQM network. The HKOMI retrieval does not change the correlation coefficient considerably compared to the standard products, while they are generally increase in other custom products (e.g. Lin et al., 2014; Russell et al., 2011; Zhou et al., 2009). The non-existent improvement has two main reasons. First, the low CTM performance can result in random errors impacting ancillary parameters and conversion factors. Second, ground-based point values were compared with satellite-based area-averaged values in an urban area with high $\mathrm{NO_2}$ variability. The expected discrepancies between ground- and satellite-based observations were estimated using CMAQ $\mathrm{NO_2}$ distributions showing that the expected correlation coefficients were quite small reducing possible improvements.

On the other hand, the HKOMI retrieval significantly reduces the bias between ground- and satellite-based observations. However, systematic errors in the parameters can still cause biases in the datasets. For example, if the model underestimates emissions, NO_2 and β_{ext} profiles might be described better by the "polluted" than the "clean" profiles (Fig. 2). As a consequence, the AMFs are reduced by about 9 % and the conversion factor by about 3 %. Therefore, NO_2 mixing ratios would be underestimated by 10 to 20 % which can partly explain the large NMB at FSGZ.

Besides these limitations, the HKOMI retrieval shows the possibility for unbiased NO_2 observations using satellite instruments. Of the four aerosol cases, HKOMI-4 performed best with the highest correlation coefficient and the smallest NMB. Furthermore, HKOMI-4 makes the most reasonable assumptions, although very simple, about aerosols and clouds. Correlation coefficients and mean biases are expected to improve further with better CTM performance.

5.4 Model evaluation and further applications

The model evaluation with OMI NO_2 datasets demonstrated that it is possible to study the spatial distribution and the magnitude of NO_2 VCDs with satellite observations. The biases between CMAQ and HKOMI-4 are consistent with the bias found between CMAQ and RAQM giving us further confidence that the HKOMI-4 retrieval results in smaller systematic errors. Small systematic errors are important for various applications.

In air quality studies, satellite observations can be used to obtain ground level NO_2 concentrations (e.g. Lamsal et al., 2008). To estimate the impact on human health, these concentrations need to be unbiased because otherwise the air quality is misinterpreted. This is particular important in polluted areas, where NO_2 VCDs can be biased due to the presence of absorbing aerosols. Our retrieval reduces this bias in particular for high NO_2 values making it more suitable for satellite-based air quality studies in urban areas.

Satellite observations can also be used for estimating NO_x emissions by inverse modelling (e.g. Mijling et al., 2013; Gu et al., 2014). Systematic errors in the satellite observations can cause biases in the derived emission inventory (e.g. Connor et al., 2008). To reduce this problem, Gu et al. (2014) derived emissions by iteratively updating the a priori NO_2 profiles used in satellite retrieval. Their method reduces differences between emissions derived from GOME-2 and OMI. However, we and other showed that NO_2 VCDs can still be biased due to surface reflectance, aerosols and clouds. Therefore, we think it is necessary to also update AKs in the inverse method and to characterise the spatiotemporal distribution of systematic errors in the satellite retrieval. The latter was done, for example, for the retrieval of carbon dioxide (Buchwitz et al., 2013).

6 Conclusions

In this paper, we evaluated biases in a regional CTM ($3\,\mathrm{km} \times 3\,\mathrm{km}$ spatial resolution) with ground- and satellite-based $\mathrm{NO_2}$ observations. Atmospheric chemistry was simulated with the CMAQ modelling system and ground measurements were taken from the RAQM network. Six OMI $\mathrm{NO_2}$ datasets were compiled with NASA's standard retrieval (OMNO2-SP and -SW) and our custom retrieval (HKOMI-1 to -4). In the OMNO2-SW dataset, a priori $\mathrm{NO_2}$ profiles were replaced by CMAQ profiles using the scattering weights provided with the product. In the HKOMI retrieval, we recalculated tropospheric AMFs using updated ancillary parameters of a priori $\mathrm{NO_2}$ profiles, surface reflectance and aerosol profiles. The HKOMI datasets differ in how aerosols were implemented in the retrieval.

The updated ancillary parameters increased tropospheric $\mathrm{NO_2}$ VCDs by $(+11.4 \pm 13.4)\,\%$ (a priori $\mathrm{NO_2}$ profiles), $(+11.0 \pm 20.9)\,\%$ (surface reflectance) and $(+6.0 \pm 8.4)\,\%$ (HKOMI-4 aerosol parametrization). As a result, the normalised mean bias (NMB) between satellite and ground observations was significantly reduced from $-41\,\%$ (OMNO2-SP) to $-15\,\%$ (HKOMI-4). The remaining biases can be explained by the CMAQ model bias and the area averaging effect due to the OMI ground pixel size. Replacing only the a priori profiles, which is recommended for model evaluation studies, only reduced the NMB to $-32\,\%$.

Since ancillary parameters have such a strong influence on the VCDs, the parameters need to be well known to obtain accurate $\mathrm{NO_2}$ VCDs and to estimate their uncertainties. In our study, $\mathrm{NO_2}$ and aerosol profile observations were not available making it difficult to estimate uncertainties and their impact on the AMF calculations. Future studies are necessary to address these limitations.

The CTM performance was low mainly due to the underestimated emissions causing a large bias in Foshan and Guangzhou (NMB $= -40\,\%$). However, the results the model evaluation with the RAQM network and the OMI $\mathrm{NO_2}$ datasets were consistent. We also estimated that our custom retrieval could still underestimate VCDs by 10 to 20 % in some areas which is important to remember when validating a model with satellite products. In general, we expect an improved HKOMI product with better CTM simulation.

To conclude, our study demonstrates that the datasets created by the HKOMI retrieval are suitable for the evaluation of the spatial distributions and the magnitudes of $\mathrm{NO_2}$ concentrations in the model. We showed that a retrieval, which updates not only a priori $\mathrm{NO_2}$ profiles, reduces the biases in urban areas. Since the ancillary parameters have a large impact on the retrieval, tools need to be developed to keep track of their influence on the final product. Such tools could improve CTM evaluations with satellite observations.

The Supplement related to this article is available online at doi:10.5194/acp-0-1-2015-supplement.

Acknowledgements. The work described in this paper is partly funded by the Guy Carpenter Asia-Pacific Climate Impact Centre (project no. 9360126), a grant from the Research Grant Council of Hong Kong (project no. 102912) and the start-up grant from City University of Hong Kong (project no. 7200296).

References

Acarreta, J. R., De Haan, J. F., and Stammes, P.: Cloud pressure retrieval using the O_2-O_2 absorption band at 477 nm, J. Geophys. Res., 109, D05204, doi:10.1029/2003JD003915, 2004.

Beirle, S., Platt, U., Wenig, M., and Wagner, T.: Weekly cycle of NO_2 by GOME measurements: a signature of anthropogenic sources, Atmos. Chem. Phys., 3, 2225–2232, doi:10.5194/acp-3-2225-2003, 2003.

Bey, I., Jacob, D. J., Yantosca, R. M., Logan, J. A., Field, B. D., Fiore, A. M., Li, Q., Liu, H. Y., Mickley, L. J., and Schultz, M. G.: Global modeling of tropospheric chemistry with assimilated meteorology: model description and evaluation, J. Geophys. Res., 106, 23073–23095, doi:10.1029/2001JD000807, 2001.

Boersma, K. F., Eskes, H. J., Meijer, E. W., and Kelder, H. M.: Estimates of lightning NO_x production from GOME satellite observations, Atmos. Chem. Phys., 5, 2311–2331, doi:10.5194/acp-5-2311-2005, 2005.

Boersma, K. F., Eskes, H. J., Veefkind, J. P., Brinksma, E. J., van der A, R. J., Sneep, M., van den Oord, G. H. J., Levelt, P. F., Stammes, P., Gleason, J. F., and Bucsela, E. J.: Near-real time retrieval of tropospheric NO_2 from OMI, Atmos. Chem. Phys., 7, 2103–2118, doi:10.5194/acp-7-2103-2007, 2007.

Boersma, K. F., Eskes, H. J., Dirksen, R. J., van der A, R. J., Veefkind, J. P., Stammes, P., Huijnen, V., Kleipool, Q. L., Sneep, M., Claas, J., Leitão, J., Richter, A., Zhou, Y., and Brunner, D.: An improved tropospheric NO_2 column retrieval algorithm for the Ozone Monitoring Instrument, Atmos. Meas. Tech., 4, 1905–1928, doi:10.5194/amt-4-1905-2011, 2011.

Bovensmann, H., Burrows, J. P., Buchwitz, M., Frerick, J., Noël, S., Rozanov, V. V., Chance, K. V., and Goede, A. P. H.: SCIAMACHY: mission objectives and measurement modes, J. Atmos. Sci., 56, 127–150, 1999.

Buchwitz, M. and Reuter, M. and Bovensmann, H. and Pillai, D. and Heymann, J. and Schneising, O. and Rozanov, V. and Krings, T. and Burrows, J. P. and Boesch, H. and Gerbig, C. and Meijer, Y. and Löscher, A.: Carbon Monitoring Satellite (CarbonSat): assessment of atmospheric CO_2 and CH_4 retrieval errors by error parameterization, Atmos. Meas. Tech., 6, 3477–3500, doi:10.5194/amt-6-3477-2013, 2013

Bucsela, E. J., Celarier, E. A., Wenig, M. O., Gleason, J. F., Veefkind, J. P., Boersma, K. F., and Brinksma, E. J.: Algorithm for NO_2 vertical column retrieval from the ozone monitoring instrument, IEEE T. Geosci. Remote, 44, 1245–1258, doi:10.1109/TGRS.2005.863715, 2006.

Bucsela, E. J., Krotkov, N. A., Celarier, E. A., Lamsal, L. N., Swartz, W. H., Bhartia, P. K., Boersma, K. F., Veefkind, J. P., Gleason, J. F., and Pickering, K. E.: A new stratospheric and tropospheric NO_2 retrieval algorithm for nadir-viewing satellite instruments: applications to OMI, Atmos. Meas. Tech., 6, 2607–2626, doi:10.5194/amt-6-2607-2013, 2013.

Burrows, J. P., Weber, M., Buchwitz, M., Rozanov, V., Ladstätter-Weißenmayer, A., Richter, A., DeBeek, R., Hoogen, R., Bramstedt, K., Eichmann, K. U., Eisinger, M. and Perner, D.: The global ozone monitoring experiment (GOME): mission concept and first scientific results, J. Atmos. Sci., 56, 151–175, 1999.

Byun, D. and Schere, K. L.: Review of the governing equations, computational algorithms, and other components of the Models-3 Community Multiscale Air Quality (CMAQ) modeling system, Appl. Mech. Rev., 59, 51–57, doi:10.1115/1.2128636, 2006.

Callies, J., Corpaccioli, E., Eisinger, M., Hahne, A., and Lefebvre, A.: GOME-2 – Metop's second-generation sensor for operational ozone monitoring, ESA Bull.-Eur. Space, 102, 28–36, 2000.

Chan, K. L., Pöhler, D., Kuhlmann, G., Hartl, A., Platt, U., and Wenig, M. O.: NO_2 measurements in Hong Kong using LED based long path differential optical absorption spectroscopy, Atmos. Meas. Tech., 5, 901–912, doi:10.5194/amt-5-901-2012, 2012.

Connor, B. J., Boesch, H., Toon, G., Sen, B., Miller, C., and Crisp, D.: Orbiting Carbon Observatory: Inverse method and prospective error analysis, J. Geophys. Res., 113, D05305, doi:10.1029/2006JD008336, 2008.

Dave, J. V.: Multiple scattering in a non-homogeneous, Rayleigh atmosphere, J. Atmos. Sci., 22, 273–279, 1965.

Dobber, M., Dirksen, R., Levelt, P., Van den Oord, G. H. J., Voors, R., Kleipool, Q., Jaross, G., Kowalewski, M., Hilsenrath, E., Leppelmeier, G., de Vries, J., Dierssen, W., and Rozemeijer, N.: Ozone monitoring instrument calibration, IEEE T. Geosci. Remote, 44, 1209–1238, doi:10.1109/TGRS.2006.869987, 2006.

Douglass, A. R., Stolarski, R. S., Strahan, S. E., and Connell, P. S.: Radicals and reservoirs in the GMI chemistry and transport model: comparison to measurements, J. Geophys. Res., 109, D16302, doi:10.1029/2004JD004632, 2004.

Driscoll, C. T., Lawrence, G. B., Bulger, A. J., Butler, T. J., Cronan, C. S., Eagar, C., Lambert, K. F., Likens, G. E., Stoddard, J. L., and Weathers, K.: Acidic deposition in the northeastern United States: sources and inputs, ecosystem effects, and management strategies, Bioscience, 51, 180–198, doi:10.1641/0006-3568(2001)051[0180:ADITNU]2.0.CO;2, 2001.

Du, Y.: New consolidation of emission and processing for air quality modeling assessment in Asia, Master's thesis, University of Tennessee, available at: http://trace.tennessee.edu/utk_gradthes/372 (last access: August 2014), 2008.

Duncan, B. N., Strahan, S. E., Yoshida, Y., Steenrod, S. D., and Livesey, N.: Model study of the cross-tropopause transport of biomass burning pollution, Atmos. Chem. Phys., 7, 3713–3736, doi:10.5194/acp-7-3713-2007, 2007.

Eskes, H. J. and Boersma, K. F.: Averaging kernels for DOAS total-column satellite retrievals, Atmos. Chem. Phys., 3, 1285–1291, doi:10.5194/acp-3-1285-2003, 2003.

Guangdong Provincial Environmental Protection Monitoring Centre (GDEMC) and Environmental Protection Department, HKSAR (HKEPD): Pearl River Delta Regional Air Quality Monitoring Network – a report of monitoring results in 2006 (PRDAIR-2006-2), available at: http://www.epd.gov.hk/epd/english/resources_pub/publications/m_report.html (last access: April 2014), 2006.

Gu, D., Wang, Y., Smeltzer, C. and Boersma, K. F.: Anthropogenic emissions of NO_x over China: Reconciling the difference of inverse modeling results using GOME-2 and OMI measurements, J. Geophys. Res., 119, 2169–8996, doi:10.1002/2014JD021644, 2014.

Guenther, A., Hewitt, C. N., Erickson, D., Fall, R., Geron, C., Graedel, T., Harley, P., Klinger, L., Lerdau, M., Mckay, W. A., Pierce, T., Scholes, B., Steinbrecher, R., Tallamraju, R., Taylor, J., and Zimmerman, P.: A global model of natural volatile organic compound emissions, J. Geophys. Res., 100, 8873–8892, doi:10.1029/94JD02950, 1995.

Haagen-Smit, A. J.: Chemistry and physiology of Los Angeles smog, Ind. Eng. Chem., 44, 1342–1346, 1952.

Han, K. M., Lee, C. K., Lee, J., Kim, J., and Song, C. H.: A comparison study between model-predicted and OMI-retrieved tropospheric NO_2 columns over the Korean peninsula, Atmos. Environ., 45, 2962–2971, doi:10.1016/j.atmosenv.2010.10.016, 2011.

Han, K. M., Lee, S., Chang, L. S., and Song, C. H.: A comparison study between CMAQ-simulated and OMI-retrieved NO_2 columns over East Asia for evaluation of NO_x emission fluxes of INTEX-B, CAPSS, and REAS inventories, Atmos. Chem. Phys., 15, 1913–1938, doi:10.5194/acp-15-1913-2015, 2015.

He, Q., Li, C., Mao, J., Lau, A. K.-H., and Chu, D. A.: Analysis of aerosol vertical distribution and variability in Hong Kong, J. Geophys. Res., 113, D14211, doi:10.1029/2008JD009778, 2008.

Herman, J. R., Celarier, E., and Larko, D.: UV 380 nm reflectivity of the Earth's surface, clouds and aerosols, J. Geophys. Res., 106, 5335–5351, doi:10.1029/2000JD900584, 2001.

Herron-Thorpe, F. L., Lamb, B. K., Mount, G. H., and Vaughan, J. K.: Evaluation of a regional air quality forecast model for tropospheric NO_2 columns using the OMI/Aura satellite tropospheric NO_2 product, Atmos. Chem. Phys., 10, 8839–8854, doi:10.5194/acp-10-8839-2010, 2010.

Hess, M., Koepke, P., and Schult, I.: Optical properties of aerosols and clouds: the software package OPAC, B. Am. Meteorol. Soc., 79, 831–844, 1998.

Huijnen, V., Eskes, H. J., Poupkou, A., Elbern, H., Boersma, K. F., Foret, G., Sofiev, M., Valdebenito, A., Flemming, J., Stein, O., Gross, A., Robertson, L., D'Isidoro, M., Kioutsioukis, I., Friese, E., Amstrup, B., Bergstrom, R., Strunk, A., Vira, J., Zyryanov, D., Maurizi, A., Melas, D., Peuch, V.-H., and Zerefos, C.: Comparison of OMI NO_2 tropospheric columns with an ensemble of global and European regional air quality models, Atmos. Chem. Phys., 10, 3273–3296, doi:10.5194/acp-10-3273-2010, 2010.

Kleipool, Q. L., Dobber, M. R., de Haan, J. F., and Levelt, P. F.: Earth surface reflectance climatology from 3 years of OMI data, J. Geophys. Res., 113, D18308, doi:10.1029/2008JD010290, 2008.

Knutsson, H. and Westin, C.-F.: Normalized and differential convolution: methods for interpolation and filtering of incomplete and uncertain data, in: Proceedings of Computer Vision and Pattern Recognition ('93), New York City, USA, 16–19 June 1993, 515–523, 1993.

Kuhlmann, G., Hartl, A., Cheung, H. M., Lam, Y. F., and Wenig, M. O.: A novel gridding algorithm to create regional trace gas maps from satellite observations, Atmos. Meas. Tech., 7, 451–467, doi:10.5194/amt-7-451-2014, 2014.

Kurosu, T. P. and Celarier, E. A.: OMIPIXCOR Readme File, available at: http://disc.sci.gsfc.nasa.gov/Aura/data-holdings/OMI/documents/v003/OMPIXCOR_README_V003.pdf (last access: August 2014), 2010.

Lamsal, L. N., Martin, R. V., van Donkelaar, A., Steinbacher, M., Celarier, E. A., Bucsela, E., Dunlea, E. J., Pinto, J. P.: Ground-level nitrogen dioxide concentrations inferred from the satellite-borne Ozone Monitoring Instrument, J. Geoph. Res., 113, D16, doi:10.1029/2007JD009235, 2008.

Leitão, J., Richter, A., Vrekoussis, M., Kokhanovsky, A., Zhang, Q. J., Beekmann, M., and Burrows, J. P.: On the improvement of NO_2 satellite retrievals – aerosol impact on the airmass factors, Atmos. Meas. Tech., 3, 475–493, doi:10.5194/amt-3-475-2010, 2010.

Levelt, P., van den Oord, G., Dobber, M., Malkki, A., Visser, H., de Vries, J., Stammes, P., Lundell, J., and Saari, H.: The ozone monitoring instrument, IEEE T. Geosci. Remote, 44, 1093–1101, doi:10.1109/TGRS.2006.872333, 2006.

Lin, J.-T., Martin, R. V., Boersma, K. F., Sneep, M., Stammes, P., Spurr, R., Wang, P., Van Roozendael, M., Clémer, K., and Irie, H.: Retrieving tropospheric nitrogen dioxide from the Ozone Monitoring Instrument: effects of aerosols, surface reflectance anisotropy, and vertical profile of nitrogen dioxide, Atmos. Chem. Phys., 14, 1441–1461, doi:10.5194/acp-14-1441-2014, 2014.

Lucht, W., Schaaf, C., and Strahler, A.: An algorithm for the retrieval of albedo from space using semiempirical BRDF models, IEEE T. Geosci. Remote, 38, 977–998, doi:10.1109/36.841980, 2000.

Malm, W., Gebhart, K., Molenar, J., Cahill, T., Eldred, R., and Huffman, D.: Examining the relationship between atmospheric aerosols and light extinction at Mount Rainier and North Cascades National Parks, Atmos. Environ., 28, 347–360, doi:10.1016/1352-2310(94)90110-4, 1994.

McLinden, C. A., Fioletov, V., Boersma, K. F., Kharol, S. K., Krotkov, N., Lamsal, L., Makar, P. A., Martin, R. V., Veefkind, J. P., and Yang, K.: Improved satellite retrievals of NO_2 and SO_2 over the Canadian oil sands and comparisons with surface measurements, Atmos. Chem. Phys, 14, 3637–3656, doi:10.5194/acp-14-3637-2014, 2014.

Mijling, B. and van der A, R. J. and Zhang, Q.: Regional nitrogen oxides emission trends in East Asia observed from space, Atmos. Chem. Phys., 13, 12003–12012, doi:10.5194/acp-13-12003-2013, 2013.

Mueller, M., Wagner, M., Barmpadimos, I., and Hueglin, C.: Two-week NO_2 maps for the City of Zurich, Switzerland, derived by statistical modelling utilizing data from a routine passive diffusion sampler network, Atmos. Environ., 106, 1 – 10, doi:10.1016/j.atmosenv.2015.01.049, 2015.

National Centers for Environmental Prediction/National Weather Service/NOAA/U.S. Department of Commerce: NCEP FNL operational model global tropospheric analyses, April 1997 to June 2007, available at: http://rda.ucar.edu/datasets/ds083.0/ (last access: December 2013), 1997.

Palmer, P. I., Jacob, D. J., Chance, K., Martin, R. V., Robert, J. D., Kurosu, T. P., Bey, I., Yantosca, R., Fiore, A., and Li, Q.: Air mass factor formulation for spectroscopic measurements from satellites: application to formaldehyde retrievals from the global ozone monitoring experiment, J. Geophys. Res., 106, 14539–14550, doi:10.1029/2000JD900772, 2001.

Platt, U. and Stutz, J.: Differential Optical Absorption Spectroscopy: Principles and Applications, Springer Verlag, Berlin Heidelberg, 2008.

Pleim, J. E. and Chang, J. S.: A non-local closure model for vertical mixing in the convective boundary layer, Atmos. Environ., 26, 965–981, doi:10.1016/0960-1686(92)90028-J, 1992.

Rozanov, A., Rozanov, V., Buchwitz, M., Kokhanovsky, A., and Burrows, J.: SCIATRAN 2.0 – a new radiative transfer model for geophysical applications in the 175–2400 nm spectral region, Adv. Space Res., 36, 1015–1019, 2005.

Rozanov, V., Kurosu, T., and Burrows, J.: Retrieval of atmospheric constituents in the uv-visible: a new quasi-analytical approach for the calculation of weighting functions, J. Quant. Spectrosc. Ra., 60, 277–299, doi:10.1016/S0022-4073(97)00150-7, 1998.

Rozanov, V. V. and Rozanov, A. V.: Differential optical absorption spectroscopy (DOAS) and air mass factor concept for a multiply scattering vertically inhomogeneous medium: theoretical consideration, Atmos. Meas. Tech., 3, 751–780, doi:10.5194/amt-3-751-2010, 2010.

Russell, A. R., Perring, A. E., Valin, L. C., Bucsela, E. J., Browne, E. C., Wooldridge, P. J., and Cohen, R. C.: A high spatial resolution retrieval of NO_2 column densities from OMI: method and evaluation, Atmos. Chem. Phys., 11, 8543–8554, doi:10.5194/acp-11-8543-2011, 2011.

Schaub, D., Boersma, K. F., Kaiser, J. W., Weiss, A. K., Folini, D., Eskes, H. J., and Buchmann, B.: Comparison of GOME tropospheric NO_2 columns with NO_2 profiles deduced from ground-based in situ measurements, Atmos. Chem. Phys/, 6, 3211–3229, doi:10.5194/acp-6-3211-2006, 2006.

Skamarock, W. C., Klemp, J. B., Dudhia, J., Gill, D. O., Barker, D. M., Duda, M. G., Huang, X.-Y., Wang, W., and Powers, J. G.: A description of the advanced research WRF Version 3, National Center for Atmospheric Research, Boulder, Colorado, USA, NCAR/TN-475+STR, doi:10.5065/D68S4MVH, 2008.

Solomon, S., Schmeltekopf, A., and Sanders, R.: On the interpretation of zenith sky absorption measurements, J. Geophys. Res., 92, 8311–8319, doi:10.1029/JD092iD07p08311, 1987.

Strahan, S. E., Duncan, B. N., and Hoor, P.: Observationally derived transport diagnostics for the lowermost stratosphere and their application to the GMI chemistry and transport model, Atmos. Chem. Phys., 7, 2435–2445, doi:10.5194/acp-7-2435-2007, 2007.

Streets, D. G., Bond, T. C., Carmichael, G. R., Fernandes, S. D., Fu, Q., He, D., Klimont, Z., Nelson, S. M., Tsai, N. Y., Wang, M. Q., Woo, J.-H., and Yarber, K. F.: An inventory of gaseous and primary aerosol emissions in Asia in the year 2000, J. Geophys. Res., 108, 8809, doi:10.1029/2002JD003093, 2003.

Tang, W., Cohan, D. S., Morris, G. A., Byun, D. W., and Luke, W. T.: Influence of vertical mixing uncertainties on ozone simulation in {CMAQ}, Atmos. Environ., 45, 2898 – 2909, doi:http://dx.doi.org/10.1016/j.atmosenv.2011.01.057, 2011.

Wanner, W., Strahler, A. H., Hu, B., Lewis, P., Muller, J.-P., Li, X., Schaaf, C. L. B., and Barnsley, M. J.: Global retrieval of bidirectional reflectance and albedo over land from EOS MODIS and MISR data: theory and algorithm, J. Geophys. Res., 102, 17143–17161, doi:10.1029/96JD03295, 1997.

Willmott, C. J.: On the validation of models, Phys. Geogr., 2, 184–194, http://www.tandfonline.com/doi/abs/10.1080/02723646.1981.10642213, 1981.

World Meteorological Organization: WMO Guide to Meteorological Instruments and Methods of Observation, World Meteorological Organization, 7th edn., Geneva, 2008.

Wu, Q., Wang, Z., Chen, H., Zhou, W., and Wenig, M.: An evaluation of air quality modeling over the Pearl River Delta during November 2006, Meteorol. Atmos. Phys., 116, 113–132, doi:10.1007/s00703-011-0179-z, 2012.

Xie, B., Fung, J. C. H., Chan, A., and Lau, A.: Evaluation of nonlocal and local planetary boundary layer schemes in the WRF model, J. Geophys. Res., 117, doi:10.1029/2011JD017080, 2012.

Yamartino, R. J.: Nonnegative, conserved scalar transport using grid-cell-centered, spectrally constrained Blackman cubics for applications on a variable-thickness mesh, Mon. Weather Rev., 121, 753–763, doi:10.1175/1520-0493(1993)121<0753:NCSTUG>2.0.CO;2, 1993.

Yarwood, G., Rao, S., Yocke, M., and Whitten, G. Z.: Updates to the Carbon Bond chemical mechanism: CB05. Final Report to the U.S. EPA, RT-0400675, available at: http://www.camx.com/publ/pdfs/cb05_final_report_120805.pdf (last access: February 2014), 2005.

Zhang, Q., Streets, D. G., Carmichael, G. R., He, K. B., Huo, H., Kannari, A., Klimont, Z., Park, I. S., Reddy, S., Fu, J. S., Chen, D., Duan, L., Lei, Y., Wang, L. T., and Yao, Z. L.: Asian emissions in 2006 for the NASA INTEX-B mission, Atmos. Chem. Phys., 9, 5131–5153, doi:10.5194/acp-9-5131-2009, 2009.

Zhang, R., Bian, Q., Fung, J. C., and Lau, A. K.: Mathematical modeling of seasonal variations in visibility in Hong Kong and the Pearl River Delta region, Atmos. Environ., 77, 803–816, doi:10.1016/j.atmosenv.2013.05.048, 2013.

Table 1. Standard set of ancillary parameters used in the AMF sensitivity study.

Ancillary Parameter	Value
solar zenith angle (SZA)	48°
viewing zenith angle (VZA)	0° (nadir)
relative azimuth angle (RAA)	180°
terrain height	0.0 km
surface reflectance	0.05
aerosol/cloud radiance fraction	0.00
temperature and pressure profiles	WRF average
NO_2 and aerosol profiles	CMAQ averages (see Fig. 2)

Table 2. Error measures used to compare observations and model. $\langle\cdot\rangle$ is the mean value and σ_x and σ_y are standard deviations.

Index of agreement (Willmott, 1981)	$\mathrm{IOA} = 1 - \frac{\sum_{i=1}^{N}(x_i - y_i)^2}{\sum_{i=1}^{N}(\lvert x_i - \langle y\rangle\rvert + \lvert y_i - \langle y\rangle\rvert)^2}$
Pearson's correlation coefficient	$r = \frac{1}{n-1}\sum_{i=1}^{N}\left(\frac{y_i - \langle y\rangle}{\sigma_y}\right)\left(\frac{x_i - \langle x\rangle}{\sigma_x}\right)$
Root mean square error	$\mathrm{RMSE} = \sqrt{\frac{1}{N}\sum_{i=1}^{N}(x_i - y_i)^2}$
Coefficient of variation of the RMSE	$\mathrm{CV} = \frac{\mathrm{RMSE}}{\langle y\rangle}$
Mean bias	$\mathrm{MB} = \frac{1}{N}\sum_{i=1}^{N}(x_i - y_i)$
Normalised mean bias	$\mathrm{NMB} = \frac{\mathrm{MB}}{\langle y\rangle}$

Zhou, Y., Brunner, D., Boersma, K. F., Dirksen, R., and Wang, P.: An improved tropospheric NO_2 retrieval for OMI observations in the vicinity of mountainous terrain, Atmos. Meas. Tech., 2, 401–416, doi:10.5194/amt-2-401-2009, 2009.

Zhou, Y., Brunner, D., Spurr, R. J. D., Boersma, K. F., Sneep, M., Popp, C., and Buchmann, B.: Accounting for surface reflectance anisotropy in satellite retrievals of tropospheric NO_2, Atmos. Meas. Tech., 3, 1185–1203, doi:10.5194/amt-3-1185-2010, 2010.

Zyrichidou, I., Koukouli, M. E., Balis, D. S., Kioutsioukis, I., Poupkou, A., Katragkou, E., Melas, D., Boersma, K., and van Roozendael, M.: Evaluation of high resolution simulated and OMI retrieved tropospheric NO_2 column densities over Southeastern Europe, Atmos. Res., 122, 55–66, doi:10.1016/j.atmosres.2012.10.028, 2013.

Table 3. Difference between OMI NO_2 datasets (level 2) due to different ancillary parameters.

Dataset	Compared to	All VCDs		10% highest VCDs		Different ancillary
		NMB[a]	CV[a]	NMB[a]	CV[a]	parameter
OMNO2-SW	OMNO2-SP	+11.4	13.4	+13.2	14.3	a-priori NO_2 profile
HKOMI-1	OMNO2-SW	+11.0	20.9	+11.3	19.4	surface reflectance[b]
HKOMI-2	HKOMI-1	+24.1	24.1	+29.9	29.9	aerosols (case 2)
HKOMI-3	HKOMI-1	+8.1	9.3	+12.2	12.5	aerosols (case 3)
HKOMI-4	HKOMI-1	+6.0	8.4	+9.8	11.2	aerosols (case 4)
HKOMI-4	OMNO2-SP	+31.0	34.0	+38.3	40.0	all

[a] in percent, [b] difference are also due to other difference between the OMNO2 and HKOMI retrieval, e.g. temperature profiles.

Table 4. The AMFs for different aerosol treatment cases for the standard parameters and profiles (Fig. 2).

Aerosol	Case 1	Case 2		Cases 3 & 4	
parametrisation		clean	polluted	clean	polluted
NO_2 clean	0.84	0.68	0.39	0.77	0.74
NO_2 polluted	0.82	0.65	0.35	0.74	0.70

Table 5. The difference between raw and processed CMAQ data due to the spatial resolution of the satellite instrument (area averaging error).

	IOA	r	MB[a]	NMB[b]	RMSE[a]	CV[b]
HK & SZ	0.54	+0.25	−4.6	−16	17.6	59
FS & GZ	0.77	+0.67	−1.6	−12	7.0	52
all stations	0.69	+0.56	−2.9	−17	9.3	54

[a] in ppbv, [b] in percent.

Table 6. OMI evaluation with the RAQM network.

Dataset	IOA	r	MB[a]	NMB[b]	RMSE[a]	CV[b]
Hong Kong and Shenzhen						
OMNO2-SP	0.31	+0.19	−17.5	−54	23.4	73
OMNO2-SW	0.34	+0.10	−13.0	−40	21.6	67
HKOMI-1	0.43	+0.24	−8.8	−27	20.6	64
HKOMI-2	0.52	+0.25	−0.7	−2	21.9	68
HKOMI-3	0.44	+0.20	−6.3	−20	20.7	64
HKOMI-4	0.45	+0.24	−7.4	−23	20.1	62
Foshan and Guangzhou						
OMNO2-SP	0.43	+0.47	−14.3	−48	20.9	71
OMNO2-SW	0.46	+0.45	−13.1	−44	20.2	68
HKOMI-1	0.48	+0.41	−10.7	−36	19.2	65
HKOMI-2	0.58	+0.42	−5.2	−18	17.8	60
HKOMI-3	0.50	+0.40	−8.5	−29	18.4	62
HKOMI-4	0.53	+0.46	−8.7	−29	17.9	60
All stations						
OMNO2-SP	0.40	+0.35	−10.7	−41	18.7	73
OMNO2-SW	0.42	+0.29	−8.2	−32	18.2	71
HKOMI-1	0.46	+0.31	−5.6	−22	18.2	71
HKOMI-2	0.53	+0.32	+0.7	+3	19.6	76
HKOMI-3	0.47	+0.29	−3.3	−13	18.6	72
HKOMI-4	0.50	+0.35	−3.9	−15	17.6	68

[a] in ppbv, [b] in percent.

Table 7. NO_2 mean values (in ppbv) at the RAQM network stations for CMAQ, network and OMI datasets.

Stations	CMAQ (raw)	CMAQ (processed)	RAQM	OMNO2 -SP	OMNO2 -SW	HKOMI -1	HKOMI -2	HKOMI -3	HKOMI -4
HKSZ	29.3	25.1	32.9	14.9	19.3	23.4	31.6	25.9	24.8
FSGZ	13.7	12.0	29.5	15.2	16.5	18.9	24.4	21.0	20.8
All stations	18.6	15.7	25.3	14.5	16.9	19.4	25.6	21.6	21.0

Table 8. Evaluation of the time series of CMAQ with OMI NO_2 VCDs in the two areas marked in Fig. 4.

Dataset	OMI Mean[a]	IOA	r	MB[a]	NMB[b]
Foshan and Guangzhou (area)					
OMNO2-SP	2.5	0.57	0.37	−0.5	−18
OMNO2-SW	2.8	0.57	0.39	−0.7	−26
HKOMI-1	3.1	0.55	0.35	−1.1	−35
HKOMI-2	4.0	0.51	0.35	−2.0	−49
HKOMI-3	3.5	0.56	0.43	−1.5	−42
HKOMI-4	3.4	0.54	0.37	−1.3	−40
Hong Kong and Shenzhen (area)					
OMNO2-SP	1.7	0.51	0.57	+1.2	+73
OMNO2-SW	2.2	0.64	0.59	+0.8	+37
HKOMI-1	2.4	0.65	0.51	+0.6	+24
HKOMI-2	3.2	0.66	0.45	−0.2	−8
HKOMI-3	2.7	0.75	0.58	+0.2	+9
HKOMI-4	2.6	0.71	0.56	+0.4	+15

[a] in 10^{16} molecules cm^{-2}, [b] in percent.

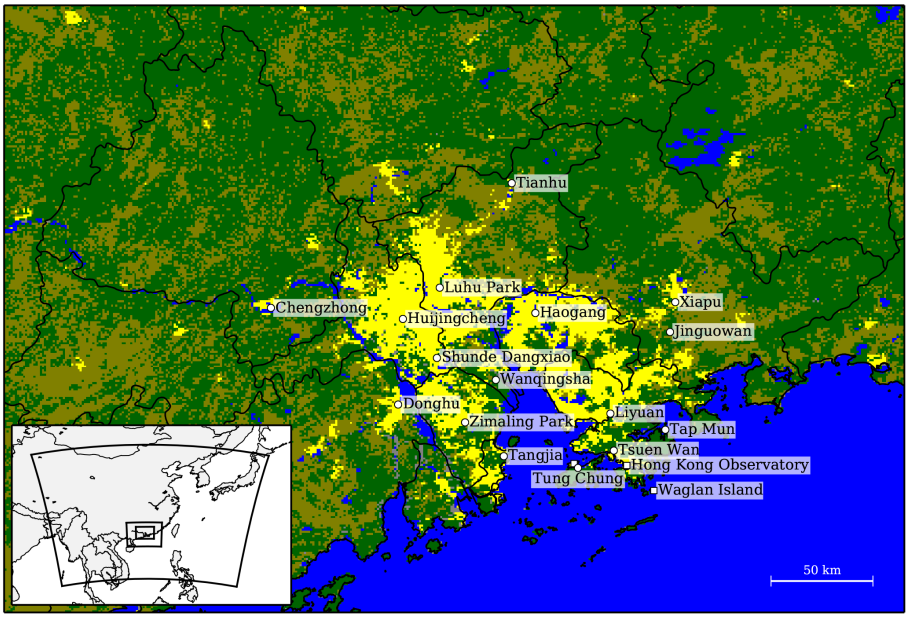

Figure 1. The large figure shows the CMAQ model domain (D3) with MODIS land categories in the Pearl River Delta (PRD) region grouped into the following categories: forest (darkgreen), crop lands (olive), bare land (grey), urban areas (yellow) and water (blue). The stations of the PRD Regional Air Quality Monitoring (RAQM) network and HKO automatic weather stations are marked by circles and squares, respectively. The small figure shows the three CMAQ model domains which are D1, D2 and D3 from the largest to smallest.

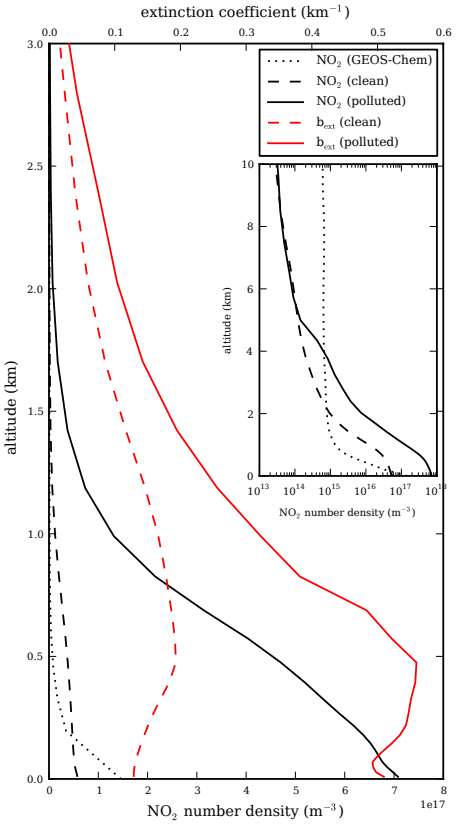

Figure 2. Averaged CMAQ NO_2 and b_{ext} profiles under "clean" and "polluted" conditions. A NO_2 profiles was categorised as polluted, if the ground number density was larger than $4.8 \times 10^{17}\,m^{-3}$ (about 20 ppbv). A b_{ext} profile was categorised as polluted, if the ground extinction coefficient was larger than 0.4. The clean b_{ext} profile has an AOT of 0.3 while the polluted as an AOT of 0.6. In addition, an annual GEOS-Chem NO_2 profile is shown for Hong Kong ($2^\circ \times 2.5^\circ$ spatial resolution).

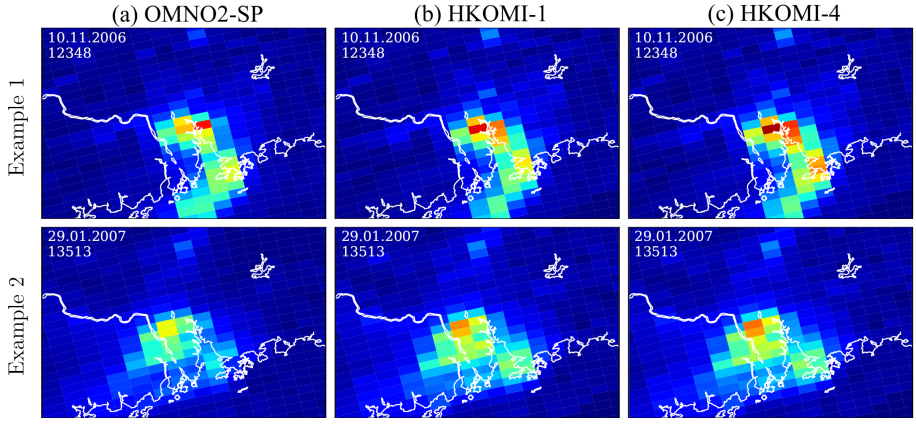

Figure 3. Two example orbits of OMI NO_2 distributions for OMNO2-SP, HKOMI-1 and HKOMI-4. The overall spatial distribution is similar but different in details. The HKOMI-1 and HKOMI-4 datasets have larger NO_2 column densities than OMNO2-SP.

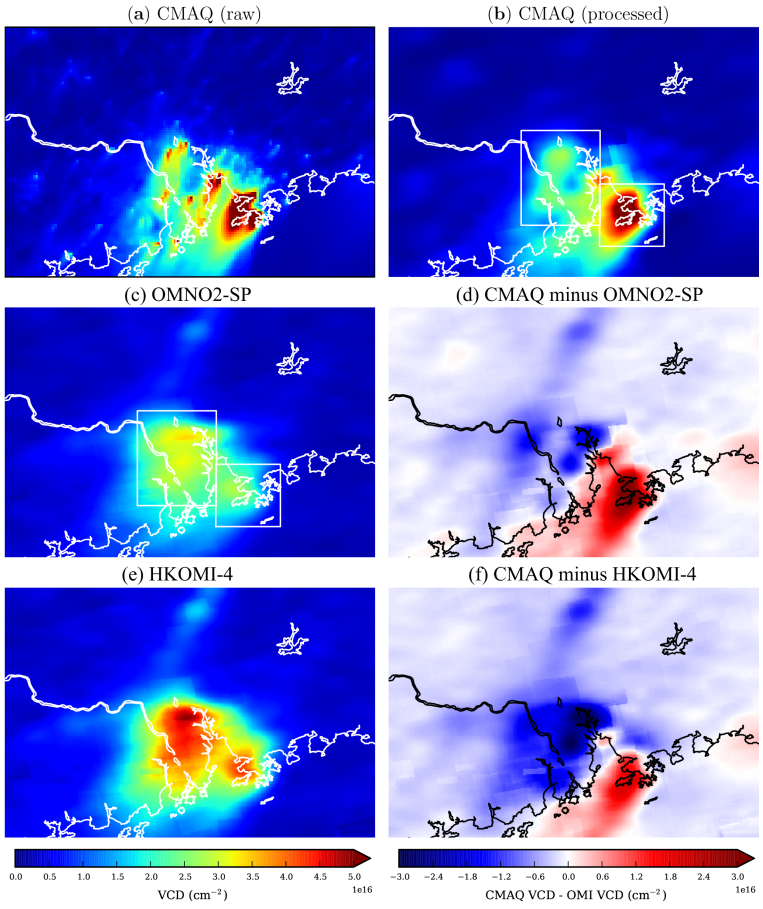

Figure 4. Four-month mean distribution of **(a)** raw and **(b)** processed CMAQ NO_2 VCDs, **(c)** OMNO2-SP VCDs and **(d)** the difference to CMAQ, **(e)** HKOMI-4 VCDs and **(f)** the difference to CMAQ.

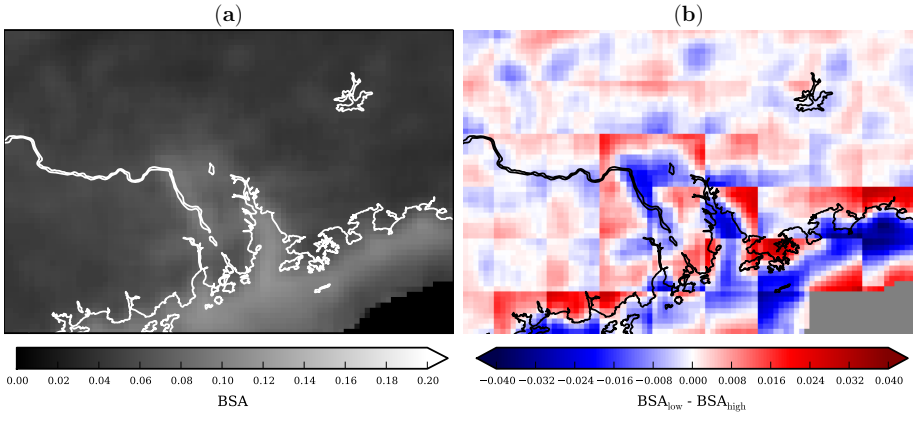

Figure 5. (a) The averaged MODIS black-sky albedo (BSA) and **(b)** the differences between low- and high-resolution BSAs.

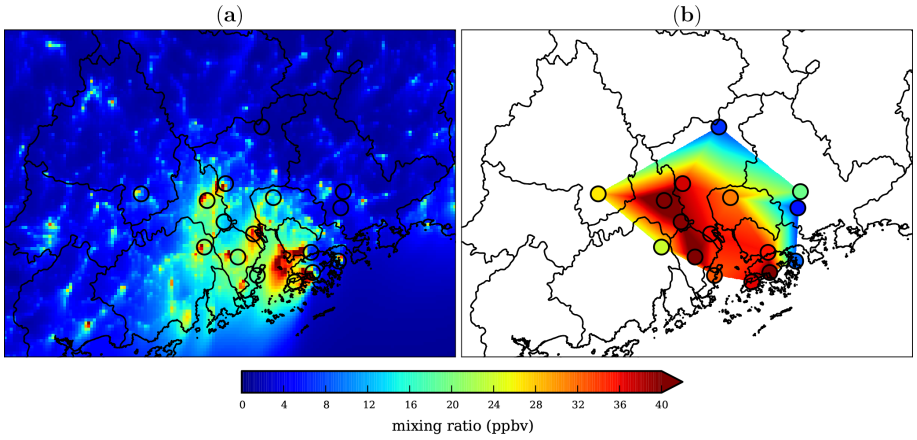

Figure 6. Ground level NO_2 mixing ratios averaged for October 2006 to January 2007: **(a)** CMAQ simulation and **(b)** RAQM network measurements. The values between stations have been estimated by linear interpolation.

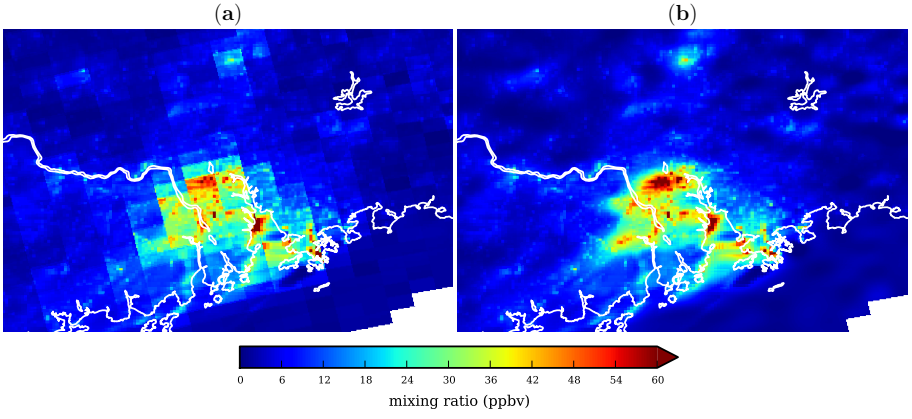

Figure 7. OMI ground mixing ratios from orbit number 13513 on 29 January 2007 comparing a **(a)** "standard" and **(b)** newly developed gridding algorithm (Kuhlmann et al., 2014). The discontinuous map created by the "standard" algorithm is difficult to interpret while the new algorithms makes an analysis of the spatial distribution easier.